Structure−Function Relationships in Human Glutathione-Dependent Formaldehyde Dehydrogenase. Role of Glu-67 and Arg-368 in the Catalytic Mechanism[†,‡]

Paresh C. Sanghani,* Wilhelmina I. Davis, LanMin Zhai, and Howard Robinson

Department of Biochemistry and Molecular Biology, Indiana University School of Medicine, Indianapolis, Indiana 46202-2111, and Biology Department, Brookhaven National Laboratory, Upton, New York 11973-5000

Received December 14, 2005; Revised Manuscript Received February 19, 2006

ABSTRACT: The active-site zinc in human glutathione-dependent formaldehyde dehydrogenase (FDH) undergoes coenzyme-induced displacement and transient coordination to a highly conserved glutamate residue (Glu-67) during the catalytic cycle. The role of this transient coordination of the active-site zinc to Glu-67 in the FDH catalytic cycle and the associated coenzyme interactions were investigated by studying enzymes in which Glu-67 and Arg-368 were substituted with Leu. Structures of FDH·adenosine 5′-diphosphate ribose (ADP-ribose) and E67L·NAD(H) binary complexes were determined. Steady-state kinetics, isotope effects, and presteady-state analysis of the E67L enzyme show that Glu-67 is critical for capturing the substrates for catalysis. The catalytic efficiency (V/K_m) of the E67L enzyme in reactions involving *S*-nitrosoglutathione (GSNO), *S*-hydroxymethylglutathione (HMGSH) and 12-hydroxydodecanoic acid (12-HDDA) were 25 000-, 3000-, and 180-fold lower, respectively, than for the wild-type enzyme. The large decrease in the efficiency of capturing GSNO and HMGSH by the E67L enzyme results mainly because of the impaired binding of these substrates to the mutant enzyme. In the case of 12-HDDA, a decrease in the rate of hydride transfer is the major factor responsible for the reduction in the efficiency of its capture for catalysis by the E67L enzyme. Binding of the coenzyme is not affected by the Glu-67 substitution. A partial displacement of the active-site zinc in the FDH·ADP-ribose binary complex indicates that the disruption of the interaction between Glu-67 and Arg-368 is involved in the displacement of active-site zinc. Kinetic studies with the R368L enzyme show that the predominant role of Arg-368 is in the binding of the coenzyme. An isomerization of the ternary complex before hydride transfer is detected in the kinetic pathway of HMGSH. Steps involved in the binding of the coenzyme to the FDH active site are also discerned from the unique conformation of the coenzyme in one of the subunits of the E67L·NAD(H) binary complex.

Human glutathione-dependent formaldehyde dehydrogenase is a class III alcohol dehydrogenase (ADH)[1] that is involved in the metabolism of nitric oxide metabolite, *S*-nitrosoglutathione (GSNO), and the adduct of formaldehyde and glutathione, *S*-hydroxymethylglutathione (HMGSH), in vivo (*1*−*3*). The oxidation product of HMGSH, *S*-formylglutathione, is further metabolized by *S*-formylglutathione hydrolase to formate and glutathione (*4*, *5*). Together, human glutathione-dependent formaldehyde dehydrogenase (FDH) and *S*-formylglutathione hydrolase form a pathway by which cells oxidize highly reactive formaldehyde to less reactive formate. A reduction of GSNO by FDH leads to the loss of a major nitrosylating agent inside the cells and constitutes a cellular strategy for regulating the signal transduction by nitric oxide inside the cells (*6*−*8*).

The unique random mechanism of FDH is in contrast to the ordered mechanism of the structurally studied eukaryotic ADHs (*9*). FDH, like other members of the mammalian ADH family, is a dimer of two identical subunits. Each of the subunits in FDH is made up of the coenzyme-binding and catalytic domains. The active site is in the cleft between the two domains and has a zinc ion that coordinates the hydroxyl and carbonyl groups of the substrates and activates them for hydride transfer. The relative position of the catalytic domain with respect to the coenzyme-binding domain controls the dimensions of the active site and plays an important role in the substrate specificity and kinetic mechanism of ADHs. The structural basis of the ordered bi-bi kinetic mechanism of class I ADHs is linked to a 10° rotation of the catalytic domain toward the coenzyme-binding domain during binding of the coenzyme to the apoenzyme (*10*). In FDH, the catalytic domain conformation is about midway between the open and closed conformations seen in class I ADH and undergoes very little change upon binding of the coenzyme (*11*). This suggests that the binding pocket for both the coenzyme and

[†] This work was supported by the Biomedical Research grant from Indiana University.

[‡] The structure factors and atomic coordinates of the FDH·ADP-ribose and E67L·NAD(H) binary complexes have been deposited in the Brookhaven Protein Data Bank under ID codes 2FZE and 2FZW, respectively.

* To whom correspondence should be addressed: Department of Biochemistry and Molecular Biology, Indiana University School of Medicine, L3-316, 1345 West 16th Street, Indianapolis, IN 46202. E-mail: psanghan@iupui.edu.

[1] Abbreviations: ADH, alcohol dehydrogenase; ADP-ribose, adenosine 5′-diphosphate ribose; FDH, human glutathione-dependent formaldehyde dehydrogenase; HMGSH, *S*-hydroxymethylglutathione; GSNO, *S*-nitrosoglutathione; 12-HDDA, 12-hydroxydodecanoic acid; 12-[$^2H_2$]-HDDA, deuterated 12-hydroxydodecanoic acid; E67L, Glu-67 to Leu substitution; R368L, Arg-368 to Leu substitution.

10.1021/bi052554q CCC: $33.50
Published on Web 03/18/2006

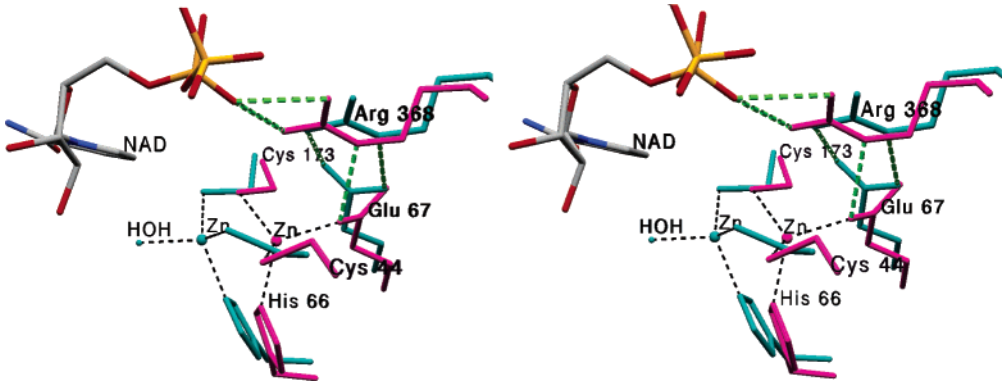

FIGURE 1: Changes in the coordination environment of the active-site zinc upon binding of the coenzyme. The relative positions of the active-site zinc and its ligands in the FDH apoenzyme (blue) and FDH·NAD(H) binary complex (pink) are shown. Only a part of the coenzyme molecule (nicotinamide ribosyl pyrophosphate portion), colored in CPK, is shown for clarity. In the view, the ribosyl ring and the pyrophosphate group are oriented toward the viewer. Binding of the coenzyme displaces the active-site zinc by 2.3 Å and increases its distance from the water molecule. The coenzyme also disrupts the bidentate interaction between Arg-368 and Glu-67 and rotates the carboxyl group of the Glu-67 toward the active-site zinc. This view was generated by initially superimposing residues 180−289 and 303−320 of the coenzyme-binding domain in the A subunit of FDH apoenzyme with the corresponding residues in the FDH·NAD(H) binary complex. All of the figures were generated using Deepview/Swiss-PdbViewer (version 3.7) and rendered using POV-Ray for Windows (downloaded from www.povray.org).

the alcohol substrate pre-exists in FDH. Structural studies also show that the active-site zinc moves back and forth between two positions during the catalytic cycle of FDH (Figure 1). In the apo form of FDH, the active-site zinc is coordinated to Cys-44, His-66, Cys-173, and a water molecule (*11*). In the FDH·NAD(H) binary complex, the active-site zinc is 2.3 Å away from its original position and substitutes the water molecule with Glu-67 in its inner coordination sphere (*12*, *13*). In the FDH·HMGSH·NAD(H) ternary complex, the active-site zinc resumed its original position and substituted Glu-67 with the hydroxyl group of HMGSH in its inner coordination sphere (*14*). Such a movement of the zinc appeared to assist ligand substitution at the active-site zinc by a double-displacement mechanism during the catalytic cycle. This observation yielded support to a proposal made by Ryde (*15*), on the basis of computational studies, that Glu-67 was assisting ligand exchange at the metal ion by moving in and out of the inner coordination sphere of the metal ion. The transient coordination of the zinc ion to a glutamate residue, as seen in FDH, could be a common phenomena in the catalytic pathway of other zinc-dependent dehydrogenases as evidenced by a growing number of enzymes reported to show zinc movement (*16*, *17*). Furthermore, the glutamate residue to which the active-site zinc coordinates transiently in FDH is a highly conserved residue not only in FDH from various species but also in all of the known zinc-dependent dehydrogenases (*18*, *19*).

The objective of this study was to examine the role and mechanism of the coenzyme-induced zinc movement in context of the structural studies on FDH. The role of zinc movement on the catalytic pathway was examined by mutating Glu-67 to leucine (E67L) and studying the effects of the mutation on the kinetic mechanism using crystallographic, initial velocity, stopped-flow, and kinetic isotope effect approaches. The mechanism by which coenzyme brings about the movement of active-site zinc was studied by evaluating the hypothesis that it was the disruption of the interaction between Glu-67 and Arg-368 that resulted in the pulling of the metal ion by Glu-67 (Figure 1). Accordingly, the zinc coordination in the FDH·adenosine 5′-diphosphate ribose(ADP-ribose) binary complex was examined, and also the effects of substituting Arg-368 to leucine on the kinetic pathway were studied.

MATERIALS AND METHODS

Materials. All of the chemicals except those noted specifically were obtained from Sigma−Aldrich Co. Monoethyl ester of dodecanedioioic acid was purchased from VWR. The chromatographic resins were purchased from Amersham Pharmacia.

Site-Directed Mutagenesis. Site-directed mutagenesis was performed using the Quick Change II site-directed mutagenesis kit from Stratagene and the pKK223-3 plasmid containing the cDNA of FDH as the starting vector. Oligonucleotides, 5′-GTGATDTTGGGACATCTAGGTGCTGGAATTGTGG-3′ and 5′-CCACAATTCCAGCACCTAGATGTCCCAAGATCAC-3′ were used as primers for generating the E67L mutation in the wild-type FDH cDNA (mutations underlined). Similarly, oligonucleotides 5′-CTGATGCATTCTGGAAAGAGCATTCTAACTGTTGTAAAGATT-3′ and 5′-AATCTTTACAACAGTTAGAATGCTCTTTCCAGAATGCATCAG-3′ were used for generating the Arg-368 to Leu substitution (R368L) mutant. The mutations were confirmed with DNA sequencing of the entire coding region of the mutant expression plasmids. BL21 cells were transformed with the mutant expression plasmids and used for expressing the enzymes.

Enzyme Expression and Purification. The wild-type and mutant enzymes were purified according to the previously described procedure with the following modifications. After the purification on DE52 and Q-sepharose chromatographic steps as previously described (*9*), the enzymes were purified using Sephacryl S-100HR and a second Q-sepharose chromatographic step. The Sephacryl S-100HR chromatography was performed using a 90 × 3.5 cm column that was operated at a flow rate of 1 mL/min. The enzyme containing fractions from the Sephacryl column were pooled and loaded on a Q-sepharose column. The enzyme was eluted from the second Q-sepharose column with a 250 mL gradient of 0−50 mM potassium phosphate at pH 7.0 containing 1 mM DTT, 10 μM $ZnSO_4$, and 1 mM benzamidine. The enzymes were

more than 90% pure as judged from SDS−PAGE analysis. The concentration of the enzyme active sites was determined by titration with NADH.

Synthesis of Deuterated 12-Hydroxydodecanoic Acid (12-[$^2H_2$]-HDDA). 12-[$^2H_2$]-HDDA was synthesized by selectively reducing the carboxylic group of the monoethyl ester of dodecanedioic acid using the method of Kanth and Periasamy (*20*). The resulting monoethylester of 12-[$^2H_2$]-HDDA was further purified by column chromatography on silica using a 7:3 mixture of dichloromethane and ethyl acetate as the developing solvent. The ester eluted near the solvent front, leaving the contaminating carboxylate compounds behind. The pure ester compound, as judged from TLC and ESI mass spectrometry, was hydrolyzed in basic solution containing methanol. 12-[$^2H_2$]-HDDA was crystallized from the mixture after evaporation of methanol and water. The final compound was evaluated by ESI mass spectrometry and found to be devoid of any contamination of the starting materials.

Steady-State and Kinetic Isotope Effect Studies Involving 12-Hydroxydodecanoic Acid (12-HDDA) and 12-[$^2H_2$]-HDDA. Initial velocity and kinetic isotope effect studies with 12-HDDA and 12-[$^2H_2$]-HDDA were performed in 0.1 M sodium glycine at pH 10 and 25 °C and involved measuring the rate of formation of NADH spectrophotometrically at 340 nm. The initial velocities were fit to the two substrate sequential mechanism using the SEQUEN program of Cleland (*21*). The isotope effects were calculated from the ratios of the constants obtained from SEQUEN fits of the data, involving 12-HDDA or 12-[$^2H_2$]-HDDA as the alcohol substrate. Inhibition experiments with dodecanoic acid were conducted as described earlier (*9*) in 0.1 M sodium glycine at pH 10 and 35 °C. The data were fit to the competitive inhibition model to get the dissociation constant of dodecanoic acid ($K_{i,dodecanoic\ acid}$).

Determination of the Equilibrium Constant for the Formation of HMGSH or [$^2H_2$]-HMGSH. The equilibrium constant for the formation of HMGSH or [$^2H_2$]-HMGSH was determined under the conditions used for the steady-state studies (50 mM potassium phosphate at pH 7.5 and 30 °C) and using the method described by Uotila and Koivusalo (*22*). The dissociation constant for the formation of HMGSH was calculated by fitting the data to eq 1.

$$\Delta F = \Delta F_M \frac{([L_T] + [E_T] + K_d) - \sqrt{([L_T] + [E_T] + K_d)^2 - 4[L_T][E_T]}}{2[E_T]} \quad (1)$$

In eq 1, ΔF is the change in the absorbance at 240 nm upon adding glutathione to formaldehyde. ΔF_M is the maximum absorbance change that was obtained from curve fitting. E_T and L_T are the concentrations of formaldehyde and glutathione, respectively. K_d is the equilibrium dissociation constant for the formation of HMGSH or [$^2H_2$]-HMGSH. The data were fitted using the Graphpad Prizm software.

Steady-State Studies Involving HMGSH and GSNO. Steady-state studies involving HMGSH and GSNO were conducted in 50 mM potassium phosphate at pH 7.5 and 30 and 25 °C, respectively. Whereas studies with HMGSH involved following the production of NADH as described above, studies with GSNO involved following the decrease in absorption at 340 nm. Because both GSNO ($\epsilon_{340} = 0.84$ mM^{-1} cm^{-1}) and NADH absorb at 340 nm and only one molecule of NADH is consumed during the reduction of GSNO, the rate of reduction of GSNO was calculated using $\epsilon_{340} = 7.06$ mM^{-1} cm^{-1} (obtained from adding the extinction coefficients of both NADH and GSNO). The concentration of HMGSH (or [$^2H_2$]-HMGSH), generated by mixing glutathione and formaldehyde (or [$^2H_2$]-HCHO), was determined from the equilibrium dissociation constant of HMGSH formation determined above. At all of the concentrations of HMGSH used in the experiments described here, the concentration of glutathione always exceeded that of formaldehyde. Specific details for a given experiment are given in the footnotes of Table 3.

Kinetic isotope effect studies with [$^2H_2$]-HMGSH were performed under the same conditions used for steady-state experiments involving HMGSH and involved a strategy similar to that used for 12-HDDA. Specific details for a given experiment are given in the footnotes of Table 4.

Equilibrium Dissociation Constant of NADH. The equilibrium dissociation constant of NADH for the wild-type FDH and the E67L and R368L enzymes was determined fluorometrically as described earlier (*9*). Binding studies were conducted in 0.1 M sodium glycine buffer at pH 10 or 50 mM potassium phosphate buffer at pH 7.5 and room temperature. During the experiment, increasing amounts of NADH were added to a 0.3−2.4 μM FDH, 0.5−1.1 μM E67L, or 3.5−5.2 μM R368L enzyme solution in a volume of 2 mL. The increase in fluorescence at 460 nm with each addition of NADH was plotted against the final concentration of NADH, and the data were fit to eq 1 using a nonlinear regression to obtain the dissociation constant of NADH.

The dissociation constant of NAD^+ for the wild-type, E67L, and R368L enzymes was also determined fluorometetrically at pH 7.5 (50 mM potassium phosphate at pH 7.5 and 23 °C) using a method described earlier (*9*). The dissociation constant was determined using a strategy similar to that used during NADH experiments described above.

Presteady-State Kinetic Studies. Stopped-flow kinetic studies were conducted using the SX18MV Applied Photophysics stopped-flow instrument with a dead time of 1 ms. During the determination of the isotope effects on the burst phase, NADH formation was monitored at 340 nm. Stopped-flow isotope effect studies with the wild-type enzyme involved mixing 52 μM FDH and 1 mM NAD^+ in 50 mM potassium phosphate at pH 7.5 with a solution of 1 mM NAD^+ and 0.55 mM HMGSH or [$^2H_2$]-HMGSH in the same buffer at 25 °C. For studies with the E67L enzyme, 14 μM E67L and 1 mM NAD^+ in 100 mM potassium phosphate at pH 7.5 were mixed with 3.65 mM HMGSH (or [$^2H_2$]-HMGSH) and 1 mM NAD^+ in the same buffer at 30 °C. The traces showing the increase in the absorbance at 340 nm were fit to eq 2 (caption of Figure 6), and the burst and the steady-state rates were calculated for each curve.

For determining the rate constants for binding and dissociation of NADH, quenching of the enzyme fluorescence ($\lambda_{exc} = 295$ nm; $\lambda_{emm} = 340$ nm) by NADH was monitored. During the determination of the association and dissociation rates of NADH for the wild-type FDH, 7.8 μM FDH in 50 mM potassium phosphate was mixed with 3.6−20 μM NADH in the same buffer at 25 °C and the quenching of the enzyme fluorescence by NADH was monitored. Studies

Table 1: Data Collection and Refinement Statistics

	FDH·ADP-ribose	E67L·NAD(H)
space group	*P*43212	*P*43212
cell parameters (a, b, c) (Å)	79.2, 79.2, 311	79.3, 79.3, 312
number of observations (total/unique)	2 160 775/79 380	2 468 590/87 472
completeness (%)	100 (100)	99.8 (99.4)
R_{merge}	9.8 (43.4)	10 (43.5)
I/σ_I	80.5 (14.1)	53.4 (9.1)
resolution (Å)	30−1.9	50−1.84
number of residues	746	746
number of zinc ions	6	4
number of water molecules	1009	1023
number of phosphate molecules	3	3
number of potassium ions	2	2
number of coenzyme or ADP-ribose molecules	2	2
R (R_{free})	18.3 (20.9)	17.8 (20.4)
rmsd for bonds (Å)	0.005	0.005
rmsd for angles (deg)	1.53	1.5

with the E67L enzyme were conducted at 30 °C and involved mixing 5.6 μM E67L with 1−14 μM NADH. The rate constants for coenzyme binding were determined by globally fitting all of the traces to the single step binding model (shown in the footnote of Table 2) using KINSIM/FITSIM.

X-ray Crystallography. The structure of the FDH·ADP-ribose binary complex was determined using the anomalous signal of zinc, whereas that of the E67L·NAD(H) complex was determined by molecular replacement using the apo form of FDH as the search model (Table 1). The crystal growth, data collection, phase determination, and refinement procedures were similar to those described earlier (*11*, *14*). Two positions of the active-site zinc in both of the subunits of the FDH·ADP-ribose binary complex became apparent from the difference Fourier maps ($F_o - F_c$) as the refinement progressed. The occupancy of the active-site zinc in each of its positions was estimated from the relative peak heights of the difference Fouriers.

RESULTS

Structures of FDH·ADP-Ribose and E67L·NAD(H) Binary Complexes. Minimal effects on the overall structure of FDH are observed upon binding of ADP-ribose or substituting Glu-67 with leucine. The space group, cell dimensions, and asymmetric unit in both the binary complexes reported here (Table 1) are similar to those observed in all of the FDH complexes showing zinc movement (*11*, *14*).

The interactions of ADP-ribose in both of the subunits of the FDH·ADP-ribose binary complex are similar to those of the adenosyl ribose moiety of NAD(H) in the FDH·NAD-(H) binary complex. An alignment of the coenzyme-binding domains in the FDH·NAD(H) and FDH·ADP-ribose binary complexes closely superimposed NAD(H) on ADP-ribose (not shown). The active-site zinc has dual occupancy in both the subunits of the FDH·ADP-ribose complex (Figure 2). The dual occupancy of the active-site zinc became apparent with refinement and was confirmed using an omit map. The coordination environment of the zinc in the first position (shown as ZnI in Figure 2), where its occupancy is about 75%, is similar to that observed in the apoenzyme (shown in Figure 1). The coordination environment of the zinc in the second position (shown as ZnII in Figure 2), where its occupancy is 25%, is similar to that in the FDH·NAD(H) binary complex (shown in Figure 1). While the zinc displacement orients the carboxyl group of Glu-67 toward the active-site zinc (Figure 1), no such changes in the conformation of Glu-67 are apparent in the FDH·ADP-ribose complex, even though the active-site zinc has 25% occupancy in its second position (ZnII in Figure 2). It is possible that, at a current resolution, there is not enough data to account for a conformational change in 25% of the Glu-67 side chains. Thus, ADP-ribose does not appear to disrupt the interaction of Glu-67 and Arg-368 as the coenzyme does and displaces the active-site zinc partly.

The active-site zinc coordinates with Cys-44, His-66, Cys-173, and a water molecule in the E67L·NADH binary complex as it does in the FDH apoenzyme (Figure 3). Substitution of Glu-67 by Leu-67 creates a void behind the active-site zinc, which is not occupied by a crystallographically ordered water molecule. Cys-173 and Leu-67 have two conformations in the A subunit of the E67L·NAD(H) binary complex (Figure 3). An evaluation of the position of the active-site zinc made by superimposing the coenzyme-binding domains of the FDH apoenzyme and the FDH·NAD-(H) and E67L·NAD(H) binary complexes shows that the position of the active-site zinc in the FDH apoenzyme and

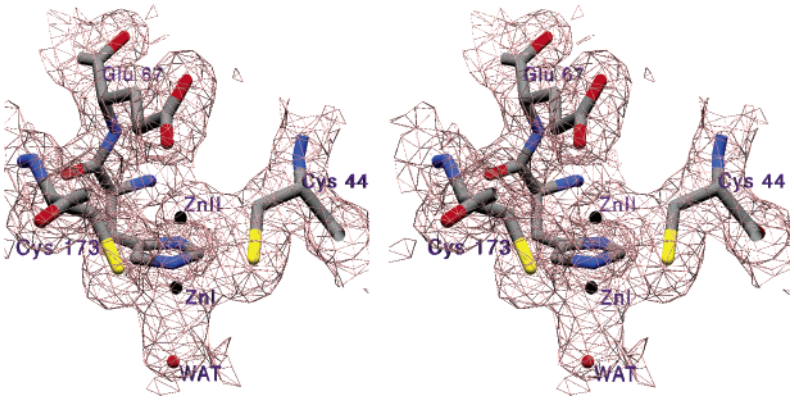

FIGURE 2: Coordination of active-site zinc in FDH·ADP-ribose binary complex. The electron density contoured at 1 standard deviation shows the coordination environment of active-site zinc. Zinc has 75% occupancy in one position (ZnI) and 25% occupancy in the other one (ZnII). The interactions of zinc in the position ZnI are similar to those seen in the FDH apoenzyme and involve coordination to Cys-173, Cys-44, His-66, and a water molecule. The interactions of zinc in its second position (ZnII) are similar to those seen in the FDH·NAD(H) binary complex. Glu-67 is 2.5 Å from the zinc and has the same conformation that it has in the FDH apoenzyme, where it interacts bidentately with Arg-368 (not shown).

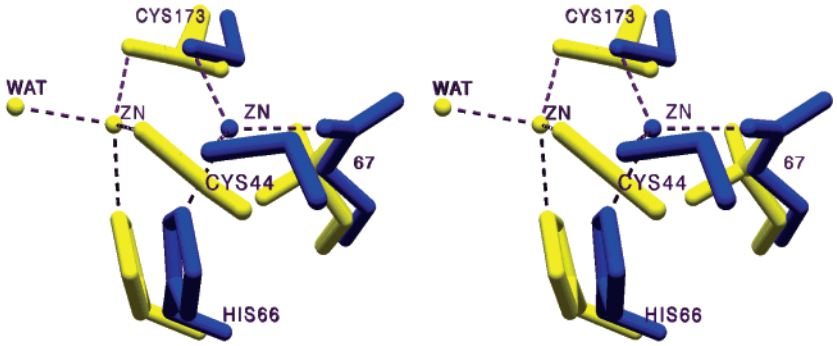

FIGURE 3: Comparison of the active-site zinc coordination in the E67L·NAD(H) and FDH·NAD(H) binary complexes. The coenzyme-binding domains of E67L·NAD(H) (yellow) and FDH·NAD(H) (blue) binary complexes were aligned as described in the caption of Figure 1. The position and the coordination environment of the active-site zinc in the E67L·NAD(H) binary complex is similar to that in the FDH apoenzyme. It is coordinated to Cys-44, His-66, Cys-173, and a water molecule. Cys-173 has two conformations, resulting from a rotation about its $C_\alpha-C_\beta$ bond. The occupancy of the sulfur in its normal position is roughly 75%, while in its other position behind the active-site zinc, its occupancy is about 25%. Leu-67 has two conformations, indicating that the side chain is rotating about the $C_\beta-C_\gamma$ bond. Mutating Glu-67 to leucine creates a void behind the active-site zinc that is not filled by any ordered water molecule.

the E67L·NAD(H) binary complex are similar. This indicates that substituting Glu-67 with Leu-67 eliminates the active-site zinc movement, presumably, because the electron-rich carboxyl group is no longer present to attract zinc.

Two conformations of the coenzyme are observed in the E67L·NAD(H) binary complex. In the A subunit, the conformation of the coenzyme is superimposable with that observed in the FDH·NAD(H) binary complex. However, in the B subunit, where the conformation and the interactions of adenosine and the pyrophosphate moieties are exactly superimposable with those of the coenzyme in the FDH·NAD(H) complex, the nicotinamide ring projects out of the active site as a result of a 190° rotation about the C4−C5 bond of the nicotinamide ribose ring (Figure 4). The hydroxyl groups of the nicotinamide ribose make hydrogen-bonding interactions with the backbone carbonyls of Val-291 and Val-293 (Figure 4). These interactions draw the loop of residues Val-290−Gly-297 into the active site and appear to hinder the nicotinamide ring from assuming its normal conformation observed in the A subunit and other FDH complexes (Figure 4). A significant puckering of the nicotinamide ring of the coenzyme is evident from the electron-density map. This is not consistent with the planar oxidized nicotinamide ring, even though the enzyme had been cocrystallized with NAD^+. Whereas the reduced state of the nicotinamide ring could account for the electron density in the B subunit (Figure 4), it could not account for the puckering in the nicotinamide ring in the A subunit. This suggested a mixture of nicotinamide rings in different oxidation states or substitutions that could not be resolved at the current resolution. Accordingly, the reduced nicotinamide ring was modeled into the electron density, although the true nature of the nicotinamide ring is not known.

Initial Velocity and Isotope Effect Studies Involving 12-HDDA at pH 10. Substituting Glu-67 with Leu significantly reduced the ability of the enzyme to catalyze the oxidation of 12-HDDA, as evident from a 66- and 183-fold decrease in the apparent second-order rate constant of the coenzyme (V/K_a) and 12-HDDA (V/K_b), respectively (Table 2). The maximal catalytic rate of 12-HDDA oxidation was also 11-fold lower in the E67L enzyme compared to the wild-type enzyme. The K_m of NAD^+ and 12-HDDA also increased by 6- and 14-fold, respectively, compared to the wild-type enzyme. Thus, the initial velocity studies show that the E67L

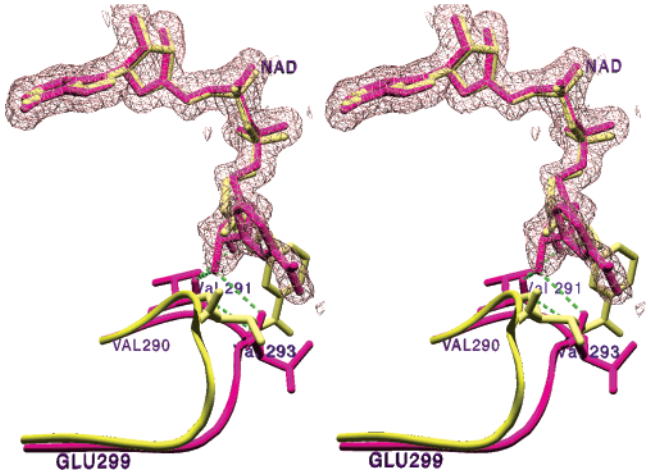

FIGURE 4: Conformation of NAD(H) in the B subunit of the E67L·NAD(H) binary complex. The coenzyme-binding domains of the B subunit of the E67L·NAD(H) and FDH·NAD(H) binary complexes were aligned as described in the caption of Figure 1 to compare the conformation of coenzyme and the nearby active-site residues in the two complexes. The nicotinamide ring of the coenzyme in the E67L·NAD(H) binary complex (purple) can assume its productive conformation seen in the FDH·NAD(H) binary complex (yellow) following a clockwise 190° rotation about its C4′−C5′ bond of the nicotinamide ribose. The loop of residues 291−295 are drawn into the NADH-binding site in the E67L·NAD-(H) binary complex (purple) as a result of a hydrogen-bonding interaction of backbone carbonyl groups of Val-291 and Val-293. The electron density ($2F_o - F_c$), contoured at 1 standard deviation, shows the conformation of the coenzyme in the E67L·NAD(H) binary complex.

enzyme is significantly impaired in capturing NAD^+ and 12-HDDA for catalysis. The effects of Glu-67 substitution appear to be more pronounced on the alcohol substrate than on the coenzyme as judged from the larger effects on the kinetic constants for 12-HDDA than for NAD^+.

The dissociation constants of NAD^+ (K_{ia}) and 12-HDDA (K_{ib}) for the E67L enzyme are 10- and 2-fold lower, respectively, than those for the wild-type enzyme (Table 2). This suggests that the NAD^+ binds tighter to the E67L enzyme, while the binding of 12-HDDA is not significantly different from that in the wild-type enzyme.

The effects of substituting Glu-67 on the substrate-binding pocket were also examined by determining the dissociation constant of the substrate analogue, dodecanoic acid. Dode-

Table 2: Kinetic Characterization of FDH and Its Mutants[a]

	FDH	E67L	R368L
Studies at pH 10			
V (min^{-1})	173 ± 4	15.7 ± 0.9	157 ± 5
K_a (μM)	9.3 ± 1.6	54 ± 8.8	160 ± 20
K_b (μM)	41 ± 7	680 ± 80	160 ± 20
V/K_a (min^{-1} μM^{-1})	19 ± 3	0.29 ± 0.04	0.98 ± 0.11
V/K_b (min^{-1} μM^{-1})	4.2 ± 0.6	0.023 ± 0.002	1.01 ± 0.12
K_{ia}	109 ± 26	15 ± 7	860 ± 160
K_{ib}	484 ± 125	190 ± 100	840 ± 160
^DV	1.9 ± 0.06	3.1 ± 0.3	3.6 ± 0.2
$^D(V/K_a)$	2.2 ± 0.5	1.7 ± 0.4	3.0 ± 0.7
$^D(V/K_b)$	4.3 ± 0.7	5.4 ± 0.5	4.4 ± 0.8
$K_{i,dodecanoic\ acid}$ (μM)	148 ± 15	617 ± 75	161 ± 20
K_{NADH} (μM)	0.98 ± 0.05	0.11 ± 0.01	3.8 ± 0.4
Studies at pH 7.5			
K_{NADH} (μM)	0.07 ± 0.02	0.076 ± 0.006	1.5 ± 0.08
K_{NAD^+} (μM)	24.6 ± 1.6	22.3 ± 2.5	273 ± 20
$k_{on,NADH}$ (M^{-1} s^{-1})	3.5 (± 0.03) × 10^7	2.2 (± 0.01) × 10^7	
$k_{off,NADH}$ (s^{-1})	3.18 ± 0.2	1.43 ± 0.12	

[a] Initial velocity and kinetic isotope effect studies were performed in 0.1 M sodium glycine buffer at pH 10 and 25 °C. Kinetic isotope effects were determined by two experiments, one conducted with 12-HDDA and another with 12-[$^2H_2$]-HDDA as the alcohol substrate. The initial velocities were fitted to the two substrate sequential mechanism using SEQUEN. K_a and K_b are Michaelis constants of NAD^+ and 12-HDDA, respectively. K_{ia} and K_{ib} are the dissociation constants of NAD^+ and 12-HDDA from their respective binary complexes and were obtained from the SEQUEN fits. ^DV, $^D(V/K_a)$, and $^D(V/K_b)$ represent the isotope effects on the maximal rate and the apparent second-order rate constant of NAD^+ and 12-HDDA, respectively. The isotope effects were determined by taking the ratio of kinetic constants of protio and deuterio substrates. Each parameter is shown with the associated standard error. $K_{i,dodecanoic\ acid}$ is the inhibition constant of dodecanoic acid that was obtained from a inhibition experiment conducted at 35 °C in 0.1 M sodium glycine at pH 10. The value of the constant with associated standard error is shown. K_{NADH} is the equilibrium dissociation constant of NADH, obtained by measuring the resonance energy transfer from the protein onto the bound NADH (λ_{exc} = 295 nm; λ_{emm} = 460 nm). The dissociation constant was measured at 25 °C in 0.1 M sodium glycine at pH 10 or in 50 mM potassium phosphate at pH 7.5. Each K_{NADH} value is an average of two minimum independent experiments and is shown with the associated standard error. K_{NAD^+} is the equilibrium dissociation constant of NAD^+ obtained by measuring the quenching of the tryptophan fluorescence of the enzyme (λ_{exc} = 300 nm; λ_{emm} = 340 nm) by NAD^+ at 25 °C in 50 mM potassium phosphate at pH 7.5. Each K_{NAD^+} value is an average of two minimum independent experiments and is shown with the associated standard error. The stopped-flow experiments were conducted in 50 mM potassium phosphate at pH 7.5 and 25 °C (for the wild-type FDH) or 30 °C (for the E67L enzyme) and involved monitoring the quenching of enzyme fluorescence by the coenzyme (λ_{exc} = 295 nm; λ_{emm} = 340 nm). Studies with wild-type FDH involved mixing 7.8 μM enzyme with 3.6−20 μM NADH, while studies with the E67L enzyme involved mixing 5.6 μM enzyme with 1−14 μM NADH. The on and off rates of the coenzyme were determined by globally fitting all of the traces to a single step binding model, $E + NADH \underset{k_{off}}{\overset{k_{on}}{\rightleftharpoons}} E{\cdot}NADH$, using KINSIM/FITSIM. The value of each constant with the associated error is shown.

canoic acid shows competitive inhibition when 12-HDDA is the varied substrate and noncompetitive inhibition when NAD^+ is the varied substrate. The structure of FDH·dodecanoic acid·NAD^+ showed dodecanoic acid extending from Arg-114 at one end of the active site to the active-site zinc in its displaced position (*11*). The dissociation constant of dodecanoic acid ($K_{i,dodecanoic\ acid}$) for the E67L enzyme is 4-fold higher than that for the wild-type enzyme (Table 2), indicating modest effects on its binding interactions with the mutant enzyme. It is possible that the long hydrophobic chain of the inhibitor is accommodated in the active site optimally when the active-site zinc is in its displaced position. Together, these data suggest that the binding of both 12-HDDA and NAD^+ are not affected greatly by the Glu-67 substitution.

Initial velocity studies on the R368L enzyme showed that Arg-368 is more important for capturing the coenzyme than 12-HDDA for catalysis as evident from a 19- versus 4-fold decrease in their respective apparent second-order rate constants (Table 2). An 8-fold increase in the dissociation constant of the NAD^+ (K_{ia}) compared to a 2-fold increase in the dissociation constant of 12-HDDA (K_{ib}), suggests that the binding of the coenzyme is affected more than that of the substrate. No change in the dissociation constant of dodecanoic acid ($K_{i,dodecanoic\ acid}$) but a 2-fold increase in the dissociation constant of 12-HDDA suggests modest effects on the interaction of the hydroxyl group within the active site upon substituting Arg-368 with Leu. A minimal effect on the V_{max} upon substituting Arg-368 with Leu indicates that the reduction in the efficiency of the capture of the coenzyme does not prevent both the substrates from binding optimally for the hydride transfer.

Kinetic isotope effect studies were performed to examine the effects of the mutations of Glu-67 and Arg-368 on the kinetic pathway of FDH. The results of the isotope effect studies using 12-[$^2H_2$]-HDDA are shown in Table 2. For the wild-type enzyme, the isotope effect on the maximal velocity (^DV) was 1.9. This suggests that the hydride-transfer step is partially rate-determining during the oxidation of 12-HDDA at pH 10. The isotope effects on the second-order rate constants of NAD^+ [$^D(V/K_a)$] and 12-HDDA [$^D(V/K_b)$] for the wild-type FDH were found to be 2.2 and 4.3, respectively. The presence of isotope effects on both V/K_a and V/K_b indicates a random mechanism. However, $^D(V/K_a)$ is significantly lower than $^D(V/K_b)$, suggesting that the coenzyme has a higher commitment to catalysis than 12-HDDA and that a preferred pathway through the FDH·NAD^+ binary complex exists in the kinetic cycle.

The isotope effects on the maximal velocity in both E67L and R368L enzymes were found to be 3.1 and 3.6, respectively. This suggests that the hydride-transfer step has become increasingly rate-determining in these mutants. Changes in the isotope effects on the second-order rate constants of both NAD^+ [$^D(V/K_a)$] and 12-HDDA [$^D(V/K_b)$] upon substituting Glu-67 or Arg-368 with Leu were statistically insignificant, indicating that the preferred pathway through the E67L·NAD^+ binary complex during the oxidation of 12-HDDA changes very little by these substitutions.

Coenzyme Binding Studies. To understand the role of Glu-67 and Arg-368 in the binding of the coenzyme, the equilibrium dissociation constant of NAD^+ and NADH (K_{NADH}) for the mutants and the wild-type enzyme were determined (Table 2). The dissociation constant of NADH was determined at pH 7.5 and 10, while the dissociation constant of NAD^+ was determined only at pH 7.5. At pH 7.5, the dissociation constant of both NAD^+ and NADH did not change significantly upon substituting Glu-67 with Leu (Table 2). However, at pH 10, the dissociation constant of NADH for the E67L enzyme is 9-fold lower than that for the wild-type FDH. This suggests that, at physiological pH, Glu-67 is not involved in the binding of the coenzyme but,

at pH 10, removal of Glu-67 increases the affinity for the coenzyme.

Substituting Arg-368 with Leu increases the dissociation constant for NAD^+ and NADH by 14- and 20-fold, respectively, at pH 7.5. At pH 10, however, the dissociation constant of NADH increased only by a factor of 2 for the R368L enzyme. This suggests that Arg-368 plays an important role in the binding of the coenzyme at pH 7.5, but at pH 10, its role is less important for the binding of the coenzyme.

Stopped-flow studies were performed on the wild-type FDH and the E67L enzyme to obtain the rate constants of NADH. NADH quenches the enzyme fluorescence by a first-order process. The on and off rate constants of NADH were obtained by globally fitting the quenching of the enzyme fluorescence by NADH to the single step binding model (shown in the footnote of Table 2) using KINSIM and FITSIM. The dissociation constant calculated from the on and off rates were in agreement with those obtained by equilibrium binding methods. The off rate of NADH from the wild-type enzyme (3.18 s^{-1}; Table 2) is 3 times higher than the turnover of HMGSH [1.04 s^{-1} reported earlier (*9*)] under the same conditions, suggesting that that the coenzyme release is partially rate-determining during the oxidation of HMGSH. On the other hand, the off rate of NADH is 15 times higher than the turnover of the 12-HDDA [0.22 s^{-1} reported earlier (*9*)], determined at the same temperature. This suggests that coenzyme release is not rate-limiting during the oxidation of 12-HDDA at pH 7.5. The off rate of NADH from the E67L enzyme (1.43 s^{-1}) is very close to the turnover of HMGSH (84 min^{-1}; Table 3) under similar conditions. This suggests that the off rate of the coenzyme is the rate-determining step in the E67L enzyme during the oxidation of HMGSH (described below).

Studies Involving HMGSH and GSNO at pH 7.5. The role of Glu-67 and Arg-368 during the oxidation and reduction of the physiological substrates of FDH, HMGSH and GSNO, respectively, was also examined using steady-state methods. Initial velocity studies with HMGSH and GSNO were conducted at 30 and 25 °C, respectively, at pH 7.5.

Steady-state kinetic studies with the E67L enzyme show that the E67L enzyme is inefficient at capturing the physiological substrates HMGSH and GSNO for catalysis. The second-order rate constants of HMGSH and GSNO for the E67L enzyme are 3000- and 25 000-fold lower than those for the wild-type enzyme (Table 3). The binding of GSNO appears to be dramatically diminished, as judged from its inability to saturate the E67L enzyme (Figure 5). A 1500-fold increase in the K_m of HMGSH also is suggestive of a similar decrease in its affinity for the E67L enzyme. The apparent maximal rate for the oxidation of HMGSH is 2-fold lower in the E67L enzyme (Table 3). This suggests that the rate-limiting step is not affected significantly by the Glu-67 substitution.

Substituting Arg-368 with Leu increases the turnover of both HMGSH and GSNO by 7-fold but does not improve the overall catalytic efficiency of the enzyme as the K_m for all of the substrates increased (Table 3). The K_m for HMGSH, GSNO, NAD^+, and NADH, increased by 20-, 35-, 4-, and 5-fold, respectively, compared to the wild-type enzyme. The larger increase in the K_m for HMGSH and GSNO compared to that of the coenzymes makes the R368L enzyme less

Table 3: Kinetic Constants for Oxidation of HMGSH and Reduction of GSNO[a]

	HMGSH			NAD^+			GSNO			NADH		
	k_{cat} (min^{-1})	K_m (μM)	k_{cat}/K_m ($min^{-1}\ \mu M^{-1}$)	k_{cat} (min^{-1})	K_m (μM)	k_{cat}/K_m ($min^{-1}\ \mu M^{-1}$)	k_{cat} (min^{-1})	K_m (μM)	k_{cat}/K_m ($min^{-1}\ \mu M^{-1}$)	k_{cat} (min^{-1})	K_m (μM)	k_{cat}/K_m ($min^{-1}\ \mu M^{-1}$)
FDH[b]	150 ± 3	1.7 ± 0.1	90 ± 5	150 ± 3	3.3 ± 0.4	45 ± 5	1760 ± 30	4.8 ± 0.3	370 ± 30	2072 ± 30	2 ± 0.2	1030 ± 100
E67L[c]	84 ± 3	2650 ± 190	0.03 ± 0.003	55 ± 2	116 ± 10	0.5 ± 0.05			0.02 ± 0.0003	ND	ND	ND
R368L[d]	1200 ± 15	38 ± 1.6	32 ± 1.4	1000 ± 13	14.4 ± 1	69 ± 4.3	12 200 ± 900	160 ± 17	75 ± 9.4	13 800 ± 500	11 ± 1.1	1250 ± 130

[a] Initial velocity studies with HMGSH and GSNO were conducted in 50 mM potassium phosphate pH 7.5 at 30 and 25 °C, respectively. Each value is an average of two independent experiments and is displayed with the associated standard error. ND not determined due to the low K_m (<1.5 μM) and the low reaction velocities. [b] The kinetic constants of HMGSH oxidation were obtained by incubating varying concentrations of HMGSH and NAD^+ with FDH and fitting the initial rates to the two substrate sequential mechanism using the SEQUEN program of Cleland. The kinetic constants of GSNO reduction were obtained by varying GSNO or NADH, keeping the other substrate at saturating levels and the data was fit to the Michaelis Menten equation. [c] During the determination of K_m of HMGSH, NAD^+ was held constant at 1 mM (~20 × K_m) and HMGSH was varied from 0.24−4.6 mM; the data was fitted to the Michaelis Menten equation. During the determination of K_m of NAD^+, HMGSH was held constant at 6 mM (~2 × K_m) and NAD^+ was varied from 1.33−400 μM; the data was fitted to the TWOONE equation using the Cleland programs (*21*). During the determination of K_m of GSNO for the E67L mutant, NADH was held constant at 200 μM and GSNO varied from 0.25−3 mM; the data was fitted to the linear equation. [d] Initial velocity studies were conducted by varying one of the substrates while keeping the unvaried substrate at saturating concentrations (10 × K_m) and the data was fitted to the Michaelis Menten equation.

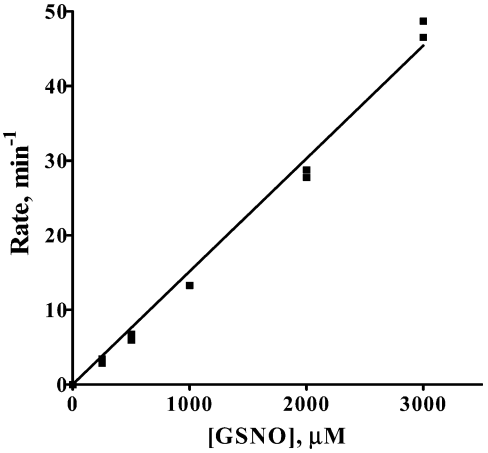

FIGURE 5: Reduction of GSNO by the E67L enzyme. The initial velocity of GSNO reduction was determined in the presence of 200 μM NADH and 3.6 μg of E67L enzyme in 50 mM potassium phosphate at pH 7.5 and 25 °C. The data were fitted to a linear equation, and the slope of the line was taken to be the apparent second-order rate constant of GSNO reduction.

Table 4: Kinetic Isotope Effects of HMGSH Oxidation by FDH Mutants[a]

	FDH[b]	E67L[c]	R368L[c]
^{D}V	1.23 ± 0.07	1.24 ± 0.07 (N)[d]	1.57 ± 0.04 (N)[d]
		1.1 ± 0.05 (H)[e]	1.59 ± 0.04 (H)[e]
$^{D}(V/K_{NAD})$	0.83 ± 0.25	1.12 ± 0.19	1.36 ± 0.14
$^{D}(V/K_{HMGSH})$	0.98 ± 0.14	1.11 ± 0.14	1.57 ± 0.12

[a] Experiments were carried out in 50 mM potassium phosphate at pH 7.5 and 30 °C. [b] Isotope effect studies involved co-incubating varying concentrations of HMGSH or [$^2H_2$]-HMGSH (0.2−10 μM) and NAD^+ (2.5−200 μM) with 1 μg of FDH and determining the initial rates; the data were fitted to the two substrate sequential mechanism equation using SEQUEN. The isotope effects were calculated by taking a ratio of the corresponding constants involving the protiated and deuterated substrate. [c] Isotope effects were determined from two parallel initial velocity experiments, in which either HMGSH (or [$^2H_2$]-HMGSH) or NAD^+ was varied, while the other substrate was held at a constant concentration. [d] NAD^+ held constant at 10 times its K_m concentration, and HMGSH or [$^2H_2$]-HMGSH was varied. [e] HMGSH held constant at a saturating concentration for the R368L mutant or at an unsaturating concentration (3.5 mM) for the E67L mutant.

efficient than the wild-type FDH in capturing these substrates for catalysis, as noted from a 3- and 5-fold decrease in their respective second-order rate constants. This suggests that Arg-368 is involved to a minor extent in capturing HMGSH and GSNO for catalysis.

Isotope effects on the steady-state constants of HMGSH were determined for FDH and the mutated enzymes to further probe the role of Glu-67 and Arg-368 in the kinetic pathway of HMGSH oxidation (Table 4). A small isotope effect is observed on the maximal rate (^{D}V) for the wild-type enzyme, indicating that the rate-determining step is not the hydride-transfer step during the oxidation of HMGSH. No isotope effects were observed on the second-order rate constants of either HMGSH or NAD^+ for the wild-type enzyme, indicating that both the substrates had a high commitment for catalysis.

The isotope effects on the steady-state constants of the E67L enzyme are similar to those observed with the wild-type enzyme. Whereas the isotope studies in which the concentration of HMGSH was varied could be carried out at a constant saturating NAD^+, it was not possible to saturate the enzyme with HMGSH, owing to its high K_m. Thus, the isotope effect on the turnover of the E67L enzyme was determined from the experiment in which NAD^+ was held at a saturating concentration and HMGSH (or [$^2H_2$]-HMGSH) was varied. This also brought $^{D}V/K_{HMGSH}$ close to its true value, whereas $^{D}V/K_{NAD}$ was not the true value. Little to no isotope effect on the maximal rate in the E67L enzyme suggest that the rate-determining step in this enzyme is not the hydride-transfer step (Table 4). A small isotope effect on the second-order rate constant of both HMGSH and NAD^+ indicate that the commitment of both the substrates is still high in the E67L enzyme.

Kinetic isotope effect studies on the R368L enzyme were conducted by varying the concentration of HMGSH (or [$^2H_2$]-HMGSH) at saturating levels of NAD^+ and vice versa. The isotope effect on the maximal rate was higher than in the wild-type enzyme, indicating that the hydride-transfer step was contributing more to the overall rate-determining step of catalysis. The isotope effects on the second-order rate constants of both the substrates also increased, suggesting a decrease in the commitments of both of the substrates.

Stopped-Flow Isotope Effects. Stopped-flow isotope effect studies were performed on the wild-type FDH and the E67L enzyme to examine whether there was an isotope effect during the presteady-state production of NADH. For the wild-type enzyme, these studies were carried out in the presence of saturating amounts of both HMGSH and NAD^+. Thus, the burst in the production of NADH observed in Figure 6A is very close to the maximal burst rate during HMGSH oxidation. A burst in the production of NADH with wild-type FDH suggests that the rate-determining step during the oxidation of HMGSH occurs after the hydride-transfer step. This is consistent with the lack of isotope effects observed on the maximal rate in the steady-state kinetic isotope effects (Table 4). The steady-state rate observed here (1.1 s^{-1} in Figure 6A) is consistent with the turnover number for oxidation of HMGSH under identical conditions [1.1 s^{-1} reported by Sanghani et al. (*9*)]. There is also a burst in the production of NADH when [$^2H_2$]-HMGSH is used as the substrate (Figure 6A). However, the burst rate constant is half of that observed with the protiated substrate (155 versus 74 s^{-1}). Hence, the hydride-transfer step is at least partially rate-limiting in the presteady-state phase of the reaction. The lack of an isotope effect during the steady-state phase of the reaction is consistent with the results in Table 4.

Determining the limiting isotope effect in the presteady-state phase of the E67L enzyme was not possible, owing to the high K_m of HMGSH. Hence, the isotope effect in the presteady state was determined using saturating and subsaturating concentrations of NAD^+ and HMGSH (or [$^2H_2$]-HMGSH), respectively. Virtually identical burst effects for NADH production are observed with subsaturating HMGSH or [$^2H_2$]-HMGSH with the E67L enzyme (Figure 6B). This suggests that a burst in the NADH production also occurs with the E67L enzyme, indicating that a step following the hydride-transfer step is rate-limiting. On the basis of the closeness of the off-rate of NADH ($k_{off,NADH}$ in Table 2) to the turnover of HMGSH (Table 3), this slowest step in the kinetic pathway of HMGSH oxidation by the E67L enzyme is likely to be the release of the coenzyme. This is also consistent with the small isotope effect on the turnover of HMGSH with the E67L enzyme (Table 4).

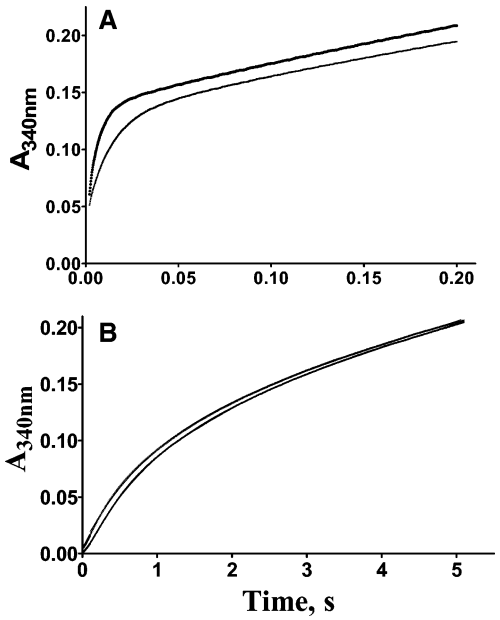

FIGURE 6: Presteady-state analysis of HMGSH oxidation by wild-type FDH and the E67L enzyme. (A) Solution containing 52 μM FDH and 1 mM NAD^+ in 50 mM potassium phosphate at pH 7.5 was mixed with a solution of 1 mM NAD^+ and 0.55 mM HMGSH (or [$^2H_2$]-HMGSH) in the stopped-flow apparatus at 25 °C, and the increase in absorbance at 340 nm was monitored. The data were fitted to eq 2: $A = A_o e^{-kt} + St + C$, using the Applied Photophysics software. A is the absorbance of the reaction mixture in the flow cell that is plotted against time t. Parameters k, S, A_o, and C are the burst rate, slope, amplitude, and constant, respectively, that are obtained from curve fitting. The steady-state rate was calculated from the slope S, using the enzyme active-site concentration (obtained from the NADH titration) and the extinction coefficient of NADH. The burst rate (k) with the protiated and deuterated HMGSH was found to be 155 ± 2.1 and 73.8 ± 0.2 s^{-1}, respectively. The steady-state rate with the protiated and deuterated HMGSH was found to be 1.1 ± 0.01 and 1.0 ± 0.002 s^{-1}, respectively. (B) Solution of 14 μM E67L enzyme and 1 mM NAD^+ in 100 mM potassium phosphate at pH 7.5 was mixed with a solution of 3.65 mM HMGSH (or [$^2H_2$]-HMGSH) and 1 mM NAD^+ in the same buffer at 30 °C, and the increase in absorbance at 340 nm was monitored. Fitting the data to eq 2 yielded a burst rate, k, of 1.09 ± 0.006 and 1.04 ± 0.005 s^{-1} for the protiated and deuterated HMGSH. The steady-state rates were found to be 0.24 ± 0.001 for the protiated and deuterated HMGSH.

Identical progress curves for NADH production with the same concentrations of HMGSH and [$^2H_2$]-HMGSH indicate that there is no isotope effect during the transient phase of HMGSH oxidation. This suggests that the hydride-transfer step is not the rate-determining step in the presteady-state phase of HMGSH oxidation by the E67L enzyme. Thus, substituting Glu-67 with Leu slows down the rate of a step before the hydride-transfer step to eliminate the isotope effect in the transient phase of NADH production.

DISCUSSION

Presence of an Isomerization Step in the Kinetic Pathway of the Oxidation of HMGSH. The burst in the production of NADH and high commitments of both of the substrates observed during the oxidation of HMGSH is not consistent with the rapid equilibrium random mechanism of FDH that had been deduced from the initial velocity studies (*9*). In a rapid equilibrium random mechanism, the substrates have a low commitment to catalysis and the rate-determining step is hydride-transfer. The results of the isotope effect studies with HMGSH would be consistent with a rapid equilibrium addition of substrates if the initial ternary complex undergoes an isomerization step that greatly increased the commitment for hydride transfer. Under this proposition, the commitments of the substrates could be low at the stage of formation of a binary complex but become high once the ternary complex is formed. The structural evidence that there is no significant domain movement upon binding of the coenzyme (or 12-HDDA) in FDH but there is a 3° domain movement upon formation of the FDH·HMGSH·NAD(H) ternary complex is consistent with the notion that an isomerization occurred in the kinetic pathway after the ternary complex is formed (*11, 14*).

The isotope effect studies on the E67L and R368L enzymes also support the isomerization step of the FDH·HMGSH·NAD^+ ternary complex. There is no increase in the $^D(V/K)$ of HMGSH, even though the binding of glutathione adducts, GSNO and HMGSH, are adversely affected in the E67L enzyme. This would happen if HMGSH has a high internal commitment factor-like isomerization of the FDH·HMGSH·NAD^+ ternary complex before the hydride-transfer step. Such a step could overcome the drop in the external commitment factor, resulting from the decrease in the affinity of HMGSH for the E67L enzyme. The small difference in the ^DV of HMGSH for the wild-type FDH and R368L enzyme, despite a 6-fold difference in their turnover (Tables 3 and 4), suggests that even after decreasing the affinity for the coenzyme by 20-fold there is still an isotope-insensitive step that is partially rate-limiting in the kinetic pathway of HMGSH oxidation in the R368L enzyme. Thus, isomerization of the FDH·HMGSH·NAD^+ ternary complex and coenzyme release are partially rate-determining steps during the oxidation of HMGSH. Inconsistency between our earlier steady-state studies (*9*) and current isotope effect studies is also observed during the oxidation of 12-HDDA. These differences, however, could have been caused by the different pH used in these studies.

Role of Glu-67 in the Kinetic Mechanism of FDH. The coordination of the active-site zinc to Glu-67 increased its distance from the water molecule and weakened their interaction (Figure 1). This appeared to facilitate ligand exchange at the active-site zinc because the incoming ligand could easily displace the loosely held water. Hence, substituting Glu-67 with Leu was expected to decrease the efficiency of the mutant enzyme in capturing the alcohol or aldehyde substrate for catalysis. Steady-state studies with the E67L enzyme concur with the structural studies and show that Glu-67 is more important for capturing the substrates, HMGSH, GSNO, and 12-HDDA, for catalysis than for the coenzyme. However, the role of Glu-67 in the kinetic pathway of 12-HDDA is different from that in the kinetic pathway of HMGSH and GSNO.

The impairment in the efficiency of the E67L enzyme in capturing GSNO and HMGSH for catalysis is contributed significantly by the reduced affinity of the mutant enzyme for these polar substrates. This is evident from the inability of GSNO to saturate the enzyme active site (Figure 5) and a suggestive, 1500-fold increase in the K_m of HMGSH (Table 3). The decrease in the efficiency of the E67L enzyme in capturing 12-HDDA, on the other hand, is not significantly different from a drop in the affinity of the mutant enzyme

for the substrate. This is evident from no effect on the dissociation constant of 12-HDDA (K_{ib} in Table 2) and a modest 4-fold increase in the dissociation constant of dodecanoate for the E67L enzyme. The reason for this difference lies in the role played by zinc coordination in the binding of these substrates. 12-HDDA is a long-chain alcohol that can bind the FDH active site without initially coordinating its hydroxyl group to the active-site zinc. This is evident from the comparable affinities of dodecanoic acid ($K_i = 33$ μM) and 12-HDDA ($K_{ia} = 69$ μM) at pH 7.5 (*9*). For HMGSH and GSNO, on the other hand, coordinating to the active-site zinc is absolutely essential for the binding, as evident from the lack of inhibition of FDH by glutathione (*9*).

The reduced efficiency of the E67L enzyme in capturing 12-HDDA for catalysis stems significantly different from the reduction in the rate of the hydride-transfer step during the oxidation of 12-HDDA. An 11-fold decrease in the turnover of 12-HDDA accompanied with significant isotope effects on the turnover suggests that the hydride-transfer step is significantly slower in the absence of Glu-67. Glu-67, however, does not play any significant role in promoting the hydride-transfer step in the kinetic pathway of HMGSH. This is evident from the lack of an isotope effect on the turnover of HMGSH by the E67L enzyme, even though there is a 2-fold decrease in it. The differential effects of Glu-67 substitution on the hydride-transfer step during the oxidation of HMGSH and 12-HDDA can be explained on the basis of altered electrostatics of the zinc environment. It is possible that, at pH 10 used for 12-HDDA studies, the water molecule is held more tightly by the active-site zinc than it would be at pH 7.5 in the E67L enzyme. The hydride-transfer step could then be occurring through a pentacoordinated zinc and be slower. Formation of a pentacoordinated zinc in the ADH active site has been reported earlier (*23*). Alternatively, it is also possible that, in the absence of Glu-67, the water molecule on the active-site zinc is never displaced by the incoming substrate. The active-site zinc, under these circumstances, would be pentacoordinated during the hydride-transfer step, with three ligands from the protein and the substrate and water molecule being the other two ligands. In the case of HMGSH and GSNO, hydride transfer may still occur efficiently because of the presence of an electronegative sulfur atom next to the C1 carbon. The hydride transfer through a pentacoordinated zinc may be slow when a primary alcohol is being oxidized.

The decrease in the efficiency of capturing the substrates by the E67L enzyme also appears to be due to a decrease in the rate at which the substrate forms a competent ternary complex that undergoes hydride transfer. No isotope effect in the presteady-state phase of HMGSH oxidation with the E67L enzyme (Figure 6B) but a significant isotope effect in the presteady phase with the wild-type enzyme suggests that a step other than hydride transfer has slowed in the absence of Glu-67. Because no significant effects on the coenzyme association are observed (Table 2), the step that slows down from the Glu-67 substitution is likely to be the association of HMGSH or the isomerization of the ternary complex before the hydride-transfer step. Similarly, the larger decrease in the second-order rate constant of 12-HDDA compared to that of NAD^+ by the E67L enzyme (Table 2) is not explained by effects on the turnover alone. In the absence of significant effects on the binding of 12-HDDA, the larger decrease in the efficiency of capturing 12-HDDA by the E67L enzyme could be ascribed to the decreased rate at which 12-HDDA forms a catalytically competent ternary complex.

A glutamate residue (Glu-68) equivalent to Glu-67 in FDH is also important for catalysis in yeast ADH, as evident from a respective 35- and 100-fold decrease in the turnover and catalytic efficiency of ethanol oxidation upon mutating it to glutamine (*24*). However, the effects on the kinetic pathway upon mutating the conserved glutamate residue are different in the yeast ADH and FDH. This could be explained by the different mutations made in the two enzymes and also could be due to the differences in the kinetic pathway of the two enzymes. The conserved glutamate is reported to be less important in *Thermoanaerobacter brockii* ADH, as evident from modest effects on the kinetic constants in the E60A mutant (*25*). Because the coordination environment of the active-site zinc is different in *T. brockii* ADH (*26*), it is possible that the role of the conserved glutamate is different in different coordination environments. Alternatively, it is also possible that the water molecule found in the void created by replacing the bulkier glutamate side chain by that of smaller alanine is partially taking the role of the carboxylate (*25*).

Role of Arg-368 in the Catalytic Cycle of FDH. Equilibrium binding studies with NAD^+ and NADH indicate that Arg-368 plays an important role in the binding of the coenzyme. However, the importance of Arg-368 in the binding of the coenzyme is influenced by Glu-67 as indicated by the pH dependence of the equilibrium binding constant of NADH. Arg-368 is less important for the binding of the coenzyme at pH 10 than at pH 7.5. The diminished role of Arg-368 in the binding of the coenzyme at higher pH can be explained by it becoming tied down by the ionized carboxyl side chain of Glu-67. This is also consistent with the observation that, in the absence of Glu-67 (E67L enzyme), the dissociation constant for NADH stays unchanged with pH, while in the presence of Glu-67 (wild-type FDH), it increases by 14-fold with pH (Table 2).

Arg-368 also assists in capturing the substrates for catalysis as evident from a 3- and 5-fold decrease in the respective catalytic efficiencies of HMGSH and GSNO, even though their turnover by the R368L enzyme is 7-fold higher. The apparent second-order rate constant of 12-HDDA is also 4-fold lower for the R368L enzyme. It is unlikely that Arg-368 substitution has altered the substrate-binding site, because the affinity of the inhibitor dodecanoic acid for the R368L enzyme is similar to that for the wild-type enzyme. It is possible that Arg-368 facilitates the capture of the substrates by steering the Glu-67 side chain into the right conformation for coordination with the active-site zinc when the coenzyme binds (Figure 1).

The partial displacement of the active-site zinc in both the active sites of the FDH·ADP-ribose binary complex suggests Arg-368 to be one of the factors that link the binding of the coenzyme to zinc movement. Whereas the active-site zinc is completely displaced in the FDH·NAD(H) binary complex (Figure 1), its partial displacement in the FDH·ADP-ribose binary complex indicates that other interactions of the coenzyme, possibly those of the nicotinamide ring, are also involved in the displacement of the active-site zinc. It is possible that the nicotinamide ring is necessary for that

small change in the conformation of the catalytic domain that moves the zinc ligands (Cys-44, His-66, and Cys-173) as the active-site zinc is being pulled by Glu-67 (Figure 1). Thus, it appears that disruption of the interaction between Arg-368 and Glu-67 changes the conformation of Glu-67 to enable it to attract the active-site zinc (Figure 1). However, the interactions of the nicotinamide ring are necessary to push the active-site zinc along with its ligands toward Glu-67.

Steps in the Binding of the Coenzyme. Steps involved in the productive binding of the coenzyme to the FDH active site can be imagined from the unique conformation of the coenzyme in the B subunit of the E67L·NAD(H) binary complex. The exposed binding pocket of the adenosine moiety and the ability of the ADP-ribose to bind FDH suggest that the preliminary event in the binding of the coenzyme is the binding of the adenosyl diphosphate moiety into the FDH active site. After the molecule was anchored by the adenosyl diphosphate, the ribose of the nicotinamide ring could interact with the backbone carbonyl groups of Val-290 and Val-293 as shown in Figure 4. Val-290 and Val-293 are on the loop of residues Val-290−Gly-297, which is quite mobile and undergoes conformational change upon binding of the coenzyme (shown in Figure 4). The loop of residues Val-290−Gly-297 could flip the unanchored nicotinamide ring into the active site as they move out of the active site (shown in Figure 4). The productive conformation of the nicotinamide ring could become stabilized by becoming sandwiched between the side chains of Val-290 and Val-293. Val-292 (equivalent to Val-293 in FDH) has been shown to be crucial in the positioning of the nicotinamide ring for hydride transfer in class I ADHs (*27*, *28*).

The proposed steps in the binding of the coenzyme are consistent with the kinetic mechanism of FDH and other ADHs having a similar structure as FDH. The release of the coenzyme from the FDH·HMGSH·NAD(H) ternary complex with its closed domain conformation is unlikely to occur, owing to the steric hindrance by the HMGSH. This would explain the preferred release of the aldehyde from FDH during the oxidative cycle and also the ordered release of aldehyde and NADH in the kinetic pathway of other ADHs (*9*, *29*−*31*). The proposed steps in the binding of the coenzyme are also consistent with an ordered binding mechanism involving the binding of the coenzyme followed by the substrate. The randomness observed in the FDH substrate addition must be possible because of the stabilization of the partial catalytic domain conformation (*11*). It must be possible for the coenzyme to swing out of the active site in the presence of the substrate, while the catalytic domain is in the partially closed conformation.

In summary, the structural and kinetic studies reported here demonstrate not only the role played by Glu-67 and Arg-368 in the FDH catalytic cycle but also give insight into the structure−function relationships in FDH and the ADH family as a whole. An isomerization of the ternary complex is evident in the kinetic pathway of FDH. During the oxidation of HMGSH, isomerization of the ternary complex and the coenzyme release are partially rate-determining. During the oxidation of 12-HDDA at pH 10, the coenzyme release and the hydride-transfer step are partially rate-determining. Glu-67 plays a key role in the catalytic efficiency of FDH, possibly by promoting the coordination of the substrate to the active-site zinc. The ability of the E67L enzyme to catalyze the oxidative and reductive reactions demonstrates that substrates are able to coordinate the active-site zinc in the absence of Glu-67. However, it is clear that, in the absence of Glu-67, the rate at which the substrate forms a productive ternary complex is significantly lower than the parent enzyme. This decrease in the rate at which the substrate associates productively with the enzyme could be due to the difficulty in displacing the zinc-bound water by the incoming substrate or the catalysis occurring through a pentacoordinated zinc.

ACKNOWLEDGMENT

We thank Drs. Bryce V. Plapp, William F. Bosron, and Thomas D. Hurley for advice and critically reading the manuscript. Ms. Jing Zhou and Udhaya Joseph are thanked for their assistance in the preparation of the mutants. The Indiana Genomics Initiative (INGEN) Protein Expression Core of Indiana University (supported in part by Lilly Endowment, Inc.) is thanked for the expression and purification of enzymes. Beamlines X25 and X29 at NSLS/Brookhaven National laboratories are thanked for high-resolution data collection.

REFERENCES

1. Koivusalo, M., Baumann, M., and Uotila, L. (1989) Evidence for the identity of glutathione-dependent formaldehyde dehydrogenase and class III alcohol dehydrogenase, *FEBS Lett. 257*, 105−109.
2. Liu, L., Hausladen, A., Zeng, M., Que, L., Heitman, J., and Stamler, J. S. (2001) A metabolic enzyme for *S*-nitrosothiol conserved from bacteria to humans, *Nature 410*, 490−494.
3. Jensen, D. E., Belka, G. K., and Du Bois, G. C. (1998) *S*-Nitrosoglutathione is a substrate for rat alcohol dehydrogenase class III isoenzyme, *Biochem. J. 331*, 659−668.
4. Koivusalo, M., Lapatto, R., and Uotila, L. (1995) Purification and characterization of *S*-formylglutathione hydrolase from human, rat and fish tissues, *Adv. Exp. Med. Biol. 372*, 427−433.
5. Uotila, L., and Koivusalo, M. (1997) Expression of formaldehyde dehydrogenase and *S*-formylglutathione hydrolase activities in different rat tissues, *Adv. Exp. Med. Biol. 414*, 365−371.
6. Liu, L., Yan, Y., Zeng, M., Zhang, J., Hanes, M. A., Ahearn, G., McMahon, T. J., Dickfeld, T., Marshall, H. E., Que, L. G., and Stamler, J. S. (2004) Essential roles of *S*-nitrosothiols in vascular homeostasis and endotoxic shock, *Cell 116*, 617−628.
7. Que, L. G., Liu, L., Yan, Y., Whitehead, G. S., Gavett, S. H., Schwartz, D. A., and Stamler, J. S. (2005) Protection from experimental asthma by an endogenous bronchodilator, *Science 308*, 1618−1621.
8. Hess, D. T., Matsumoto, A., Kim, S. O., Marshall, H. E., and Stamler, J. S. (2005) Protein S-nitrosylation: Purview and parameters, *Nat. Rev. Mol. Cell. Biol. 6*, 150−166.
9. Sanghani, P. C., Stone, C. L., Ray, B. D., Pindel, E. V., Hurley, T. D., and Bosron, W. F. (2000) Kinetic mechanism of human glutathione-dependent formaldehyde dehydrogenase, *Biochemistry 39*, 10720−10729.
10. Colonna-Cesari, F., Perahia, D., Karplus, M., Eklund, H., Braden, C. I., and Tapia, O. (1986) Interdomain motion in liver alcohol dehydrogenase. Structural and energetic analysis of the hinge bending mode, *J. Biol. Chem. 261*, 15273−15280.
11. Sanghani, P. C., Robinson, H., Bosron, W. F., and Hurley, T. D. (2002) Human glutathione-dependent formaldehyde dehydrogenase. Structures of apo, binary and inhibitory ternary complexes, *Biochemistry 41*, 10778−10786.
12. Sanghani, P. C., Robinson, H., Bennett-Lovsey, R., Hurley, T. D., and Bosron, W. F. (2003) Structure−function relationships in human class III alcohol dehydrogenase (formaldehyde dehydrogenase), *Chem.-Biol. Interact. 143*−*144*, 195−200.
13. Yang, Z. Y., Bosron, W. F., and Hurley, T. D. (1997) Structure of human $\chi\chi$ alcohol dehydrogenase: A glutathione-dependent formaldehyde dehydrogenase, *J. Mol. Biol. 265*, 330−343.
14. Sanghani, P. C., Bosron, W. F., and Hurley, T. D. (2002) Human glutathione-dependent formaldehyde dehydrogenase. Structural

changes associated with ternary complex formation, *Biochemistry 41*, 15189−15194.
15. Ryde, U. (1995) On the role of Glu-68 in alcohol dehydrogenase, *Protein Sci. 4*, 1124−1132.
16. Esposito, L., Bruno, I., Sica, F., Raia, C. A., Giordano, A., Rossi, M., Mazzarella, L., and Zagari, A. (2003) Crystal structure of a ternary complex of the alcohol dehydrogenase from *Sulfolobus solfataricus*, *Biochemistry 42*, 14397−14407.
17. Pauly, T. A., Ekstrom, J. L., Beebe, D. A., Chrunyk, B., Cunningham, D., Griffor, M., Kamath, A., Lee, S. E., Madura, R., Mcguire, D., Subashi, T., Wasilko, D., Watts, P., Mylari, B. L., Oates, P. J., Adams, P. D., and Rath, V. L. (2003) X-ray crystallographic and kinetic studies of human sorbitol dehydrogenase, *Structure 11*, 1071−1085.
18. Vallee, B. L., and Auld, D. S. (1990) Zinc coordination, function, and structure of zinc enzymes and other proteins, *Biochemistry 29*, 5647−5659.
19. Vallee, B. L., and Auld, D. S. (1990) Active-site zinc ligands and activated H_2O of zinc enzymes, *Proc. Natl. Acad. Sci. U.S.A. 87*, 220−224.
20. Kanth, J. V. B., and Periasamy, M. (1991) Selective reduction of carboxylic acids into alcohols using $NaBH_{4\ and\ I2}$, *J. Org. Chem. 56*, 5964−5965.
21. Cleland, W. W. (1979) Statistical analysis of enzyme kinetic data, *Methods Enzymol. 63*, 103−138.
22. Uotila, L., and Koivusalo, M. (1974) Formaldehyde dehydrogenase from human liver. Purification, properties, and evidence for the formation of glutathione thiol esters by the enzyme, *J. Biol. Chem. 249*, 7653−7663.
23. Boiwe, T., and Branden, C. I. (1977) X-ray investigation of the binding of 1,10-phenanthroline and imidazole to horse-liver alcohol dehydrogenase, *Eur. J. Biochem. 77*, 173−179.
24. Ganzhorn, A. J., and Plapp, B. V. (1988) Carboxyl groups near the active site zinc contribute to catalysis in yeast alcohol dehydrogenase, *J. Biol. Chem. 263*, 5446−5454.
25. Kleifeld, O., Shi, S. P., Zarivach, R., Eisenstein, M., and Sagi, I. (2003) The conserved Glu-60 residue in *Thermoanaerobacter brockii* alcohol dehydrogenase is not essential for catalysis, *Protein Sci. 12*, 468−479.
26. Korkhin, Y., Kalb, G., Peretz, M., Bogin, O., Burstein, Y., and Frolow, F. (1998) NADP-dependent bacterial alcohol dehydrogenases: Crystal structure, cofactor-binding and cofactor specificity of the ADHs of *Clostridium beijerinckii* and *Thermoanaerobacter brockii*, *J. Mol. Biol. 278*, 967−981.
27. Rubach, J. K., Ramaswamy, S., and Plapp, B. V. (2001) Contributions of valine-292 in the nicotinamide binding site of liver alcohol dehydrogenase and dynamics to catalysis, *Biochemistry 40*, 12686−12694.
28. Rubach, J. K., and Plapp, B. V. (2003) Amino acid residues in the nicotinamide binding site contribute to catalysis by horse liver alcohol dehydrogenase, *Biochemistry 42*, 2907−2915.
29. Charlier, H. A., Jr., and Plapp, B. V. (2000) Kinetic cooperativity of human liver alcohol dehydrogenase $\gamma(2)$, *J. Biol. Chem. 275*, 11569−11575.
30. Sekhar, V. C., and Plapp, B. V. (1988) Mechanism of binding of horse liver alcohol dehydrogenase and nicotinamide adenine dinucleotide, *Biochemistry 27*, 5082−5088.
31. Light, D. R., Dennis, M. S., Forsythe, I. J., Liu, C. C., Green, D. W., Kratzer, D. A., and Plapp, B. V. (1992) α-Isoenzyme of alcohol dehydrogenase from monkey liver. Cloning, expression, mechanism, coenzyme, and substrate specificity, *J. Biol. Chem. 267*, 12592−12599.

BI052554Q